DEVELOPMENT OF AN LED ARRAY FOR DOSIMETRY IN DIAGNOSTIC RADIOLOGY

EDRINE DAMULIRA

UNIVERSITI SAINS MALAYSIA

2021

DEVELOPMENT OF AN LED ARRAY FOR DOSIMETRY IN DIAGNOSTIC RADIOLOGY

by

EDRINE DAMULIRA

Thesis submitted in fulfillment of the requirements

for the degree of

Doctor of Philosophy

August 2021

ACKNOWLEDGEMENT

I dedicate this thesis to my beloved Mother the Late Harriet Najjemba Lutaaya, my True Hero. I am who I am today because of You. May Your Soul Rest in Peace, Mummy. I give honor, praise and thanks to the Almighty God for having led me through my PhD journey from the start until the end. I greatly appreciate my main supervisor Dr. Muhammad Nur Salihin Yusoff for the immense efforts, advice, suggestions, mentorship, and guidance throughout this pursuit. I also extended my sincere gratitude to my co-supervisors Dr. Ahmad Fairuz Omar and Dr. Nur Hartini Mohd Taib for their continuous reviews, comments, and suggestions about my work. I'm very grateful to my supervisors for the pivotal role played towards the nurturing of my intellectual curiosity and my growth as an independent researcher. I acknowledge the Department of Radiology, School of Medical Sciences USM, and the Engineering Physics Laboratory, School of Physics USM for facilitating the execution of all the experiments in this study by proving equipment including X-ray machines and spectrometers, respectively. I also profoundly acknowledge the Short-Term Grant, Universiti Sains Malaysia (Grant number: 304/PPSK/6315117) for funding my project. To my dear and loving family and siblings; Lydia Nantongo, Augustine Semakula, Judith Janice Nankinga, and Jackie Ntege, it would not have been all possible had it not been for your unconditional support of all kinds. Many thanks to all the anonymous reviewers for their contributions to the peer review of my thesis publications. Special thanks to Nashrulhaq Tagiling for assisting me with the thesis abstract translation to Bahasa Melayu. I also thank the Medical Radiation lab's supporting staff for their assistance, and my lab mates for all the constructive scientific and social discussions and experiences we've had and shared.

TABLE OF CONTENT

LIST OF TABLES

LIST OF FIGURES

LIST OF SYMBOLS

Z	Atomic number
e	Charge of an Electron (-1.6×10^{-19}C)
η	Eta – Refractive index
λ	Lambda – Wavelength
ϵ	Lunate Epsilon
μ	Mu – micro/mean
ν	Nu – Frequency
Ω	Omega – Resistance (Ohms)
ε	Permittivity
ε_o	Permittivity of free space
Φ	Phi
Ψ	Psi
h	Planck's constant (6.62607015×10^{-34} J·s)
σ	Sigma – Lowercase (Standard deviation)
Σ	Sigma – Uppercase (Summation)
c	Speed of light in a vacuum (2.998×10^{8}m/s)
τ	Tau
$	United States Dollar

LIST OF ABBREVIATIONS

a-Si:H	Amorphous Silicon
a-SiC	Amorphous Silicon Carbide
AC	Alternating Current
ADC	Analog to Digital Converter
ALARA	As Low as Reasonably Achievable
AlGaAs	Aluminum Gallium Arsenide
AlGaInP	Aluminum Gallium Indium Phosphide
BFPs	Blue Fluorescence Photons
BJT	Bipolar Junction Transistor
CCD	Charge Coupled Devices
CdTe	Cadmium Telluride
CE	Cherenkov Emission
CL	Cherenkov Luminescence
CLI	Cherenkov Luminescence Imaging
CMOS	Complementary Metal Oxide Semiconductor Devices
COB	Chip on Board
CT	Computed Tomography
D max	Maximum depth dose
DC	Direct Current
E	Electric Field
EMR	Electromagnetic Radiation
EMS	Electromagnetic Spectrum
EPID	Electronic Portal Imaging Device
FB	Forward Biased

GaAs	Gallium Arsenide
GaAsP	Gallium Arsenide Phosphide
GaN	Gallium (III) Nitride
Gy	Gray
HBQ	High Beam Quantity
HVL	Half Value Layer
I	Current
IGRT	Image Guided Radiation Therapy
J	Joule
kV	Kilovoltage
keV	Kilo electron volt
kVp	Kilovoltage peak
LaOBr	Lanthanum Oxybromide
LAP	LED Array Prototype
LBQ	Low beam quantity
LED	Light – emitting diode
LET	Linear Energy Transfer
LINAC	Linear accelerator
mA	Milli Ampere
MU	Monitor Unit
mV	millivolt
MeV	Mega electron volts
MOSFET	Metal-oxide-semiconductor field effect transistor
mV	millivolt
MV	Megavoltage

OSL	Optical Stimulated Luminescence
PDD	Percentage Depth Dose
Q	Charge
QA	Quality Assurance
QC	Quality Control
QE	Quantum Efficiency
R^2	R-Square
RADFET	Radiation sensitive field effect transistor
RB	Reverse Biased
RIC	Radiation-Induced Current
RF	Radio Frequency
RFW	Radio Frequency Waves
RG	Recombination-Generation
Si	Silicon
SiC	Silicon Carbide
SID	Source to Image Distance
SDD	Source to Detector Distance
SSD	Source to Surface Distance
SVWAD	Sensitivity Variation With Accumulated Dose
TLD	Thermoluminescence Dosimeter
UV	Ultraviolet
V	Volt/Potential difference/Voltage
VDMOSFET	Vertical double diffused metal oxide semiconductor field effect transistor
YAG phosphor	Yttrium aluminum garnet phosphor

PEMBANGUNAN SATU TATASUSUNAN LED UNTUK DOSIMETRI DALAM RADIOLOGI DIAGNOSTIK

ABSTRAK

Matlamat pertama penyelidikan ini adalah untuk meneroka tindak balas dosimetrik peranti pemasangan permukaan (SMD) diod pemancar cahaya (LED) terhadap sinar-X diagnostik dan alur radioterapi. Tindak balas terhadap sinar-X diagnostik diperiksa menggunakan lima warna jalur LED berdasarkan parameter sinar-X diagnostik yang berubah-ubah, termasuk puncak kilovoltan (kVp), produk arus-tiub (mAs), dos, dan jarak sumber ke pengesan. Tindak balas terhadap alur radioterapeutik pada awalnya diselidiki menggunakan LED putih sejuk, dengan mengubah sudut penyinaran, tenaga pancaran, jarak permukaan-sumber, ukuran medan, dan dos yang diserap. Objektif kedua kajian ini adalah untuk memperkuat isyarat yang terhasil dari pancaran sinar-X diagnostik dengan meningkatkan bilangan cip LED dan menggunakan papan penguat. Selain itu, perbandingan keupayaan pengesanan antara LED putih sejuk dan fotodiod bpw43 dikemukakan. Akhir sekali, penyelidikan ini bertujuan untuk mereka bentuk dan memasang sistem dosimetrik prototaip jajaran LED (LAP). LAP ini merangkumi jajaran cip LED putih sejuk fotovoltaik berukuran 20×20 cm^2 yang dilapisi di antara dua skrin penguat. Sistem ini diletakkan di dalam rongga udara yang terlindung dari gangguan optik menggunakan pita vinil hitam. Skrin tersebut menukar sinar-X diagnostik menjadi cahaya biru pendarfluor. LED itu dikendalikan dalam mod pengesan; oleh itu, LED akan mengubah cahaya pendarfluor menjadi arus yang terhasil dari radiasi. Arus analog ini dikuantifikasi dan diubah menjadi isyarat voltan digital menggunakan multimeter digital. Pencirian LAP dilaksanakan dengan (i) kualiti alur yang ditetapkan oleh IEC 61267, iaitu, RQR 7 (90

kVp) dan RQR 8 (100 kVp), dan (ii) rendah (25 mAs) dan tinggi (80 mAs) kuantiti alur ditentukan di sini. LED putih sejuk menunjukkan tingkah balas dosimetrik yang lebih baik. Peningkatan bilangan cip LED menghasilkan pekali penguat yang lebih tinggi daripada papan penguat. Kedua-dua fotodiod dan LED menunjukkan ketepatan isyarat, kelinearan terhadap mAs (dos), dan pergantungan terhadap dos dan tenaga yang serupa. Dos minimum yang dikesan oleh LAP adalah 0.1386 mGy, manakala dos maksimum yang digunakan di sini ialah ~ 13 mGy. Sementara kelinearan dos yang diserap LAP adalah 99.18%, kelinearan mAs adalah 98.64%. Sensitiviti sistem ini berubah-ubah pada ± 4.69%, ± 6.8%, dan ± 7.7% mengikut tenaga, dos, dan variasi kadar dos. Dua set data LAP adalah 89.93% boleh ulang. Oleh itu, kajian ini mencadangkan sistem prototaip dosimetrik berasaskan LED yang ultra nipis (5 mm), ringan (130 g), dan kos yang relatif rendah (US $ 255). Mekanisme dosimetrik prototaip ini adalah mudah, cekap, dan tepat.

DEVELOPMENT OF AN LED ARRAY FOR DOSIMETRY IN DIAGNOSTIC RADIOLOGY

ABSTRACT

The first goal of this research is to explore the dosimetric response of surface mount device (SMD) light-emitting diodes (LEDs) to diagnostic X-rays and radiotherapy beams. The response to diagnostic X-rays was examined using five LED strips colors based on variable diagnostic X-ray parameters, including kilovoltage peak (kVp), tube current-time product (mAs), dose, and source to detector distance. The response to radiotherapeutic beams was preliminarily investigated with a cold white LED, while varying the irradiation angle, beam energy, source-surface distance, field size, and absorbed dose. This work's second objective is to amplify diagnostic X-ray radiation-induced signals by increasing the number of LED chips and using an amplifier board. Additionally, a detection capability comparison between the cold white LED and a bpw43 photodiode is presented. Finally, this investigation aims at designing and fabricating an LED array prototype (LAP) dosimetric system. The LAP comprises a 20 × 20 cm^2 array of photovoltaic cold white LED chips sandwiched between two intensifying screens. The system was placed inside an air cavity shielded from optical noise using black vinyl tape. The screens converted diagnostic X-ray beams to fluorescent blue light. The LEDs herein were executed in detector mode; thus, they converted the fluorescent light into radiation-induced currents. These analog currents were quantified and converted into digital voltage signals using a digital multimeter. LAP characterization was implemented with (i) beam qualities established by the IEC 61267, i.e., RQR 7 (90 kVp) and RQR 8 (100 kVp), and (ii) low (25 mAs) and high (80 mAs) beam quantities defined herein. The cold white LED demonstrated

a better dosimetric behavior. LED chip number increment produced higher amplification coefficients than the amplifier board. Both the photodiode and LEDs demonstrated similar signal precision, linearity to mAs (dose), and dose and energy dependence. The minimum dose detected by the LAP was 0.1386 mGy, whereas the maximum dose implemented here was ~ 13 mGy. Whereas the LAP absorbed dose linearity was 99.18 %, mAs linearity was 98.64 %. The sensitivity of the system fluctuated by ± 4.69 %, ± 6.8 %, and ± 7.7 % during energy, dose, and dose rate variation, respectively. Two LAP data sets were 89.93 % repeatable. Thus, this study proposed an ultrathin (5 mm), lightweight (130 g), and relatively low cost (US $255) LED-based dosimetric prototype system. This prototype's dosimetric mechanism was simple, efficient, and accurate.

CHAPTER 1

INTRODUCTION

1.1 Background of the Study

Radiation could be broadly divided into charged (ionizing) and uncharged (indirectly-ionizing) radiation (Dance *et al.*, 2014). Charged particle radiation consists of fast electrons and heavy charged particles (Knoll, 2000; Dance *et al.*, 2014). On the other hand, uncharged radiation comprises electromagnetic radiation (X- and γ-ray, ultraviolet, visible spectrum, infrared, microwaves, and radio waves) and neutrons (Knoll, 2000; Dance *et al.*, 2014). In radiation spectroscopy, both the charged and uncharged radiation types interact with matter in different ways. Hence, there is essence for radiation measurement and monitoring, to control its effects in matter accordingly.

X-rays have a shorter wavelength than ultraviolet light, but longer than that of gamma (γ) rays. As electromagnetic waves, X-rays exist in the form of discrete energy packets known as photons. However, X-rays are ionizing (indirectly ionizing) electromagnetic radiation (Garcia-Sanchez *et al.*, 2018). Thus, X-rays ionize the matter they interact with by creating positive and negative charges. Owing to quantization of X-rays, X-ray photons could be characterized as high-energy particles.

Latest advancements in medicine employ radiation for executing radiotherapeutic and imaging procedures such as computed tomography (CT) (Hofstetter *et al.*, 2011). However, precaution has to be taken during radiation application. This is because excessive radiation attenuation by human tissue might result into high patient absorbed dose values (Rivera-Montalvo, 2014; Kron, Lehmann and Greer, 2016). Eventually, high patient absorbed dose could lead to development

of secondary malignancies (cancers) (Richardson *et al.*, 2015; Kron, Lehmann and Greer, 2016). Thus, there ought to be implementation of stringent measures to manage and control both intentional and unintentional radiation exposures – through medical radiation dosimetry.

Of recent, a multitude of studies (Paschoal, Souza and Santo, 2011; Romei *et al.*, 2015; Nazififard, Suh and Mahmoudieh, 2016; Oliveira, Khoury and Santos, 2016; Paschoal *et al.*, 2016; Posar *et al.*, 2020) has deployed photonic devices, in the form of photodiodes, for dosimetry in diagnostic radiology and radiation oncology. Photonic devices are electronic components fabricated and implemented for emitting, detecting, or manipulating light. Other studies (Kainka, 2011; Oliver, 2011; Anđelković and Ristić, 2013) have also exploited photodiodes for measuring and detecting gamma radiation. However, Andjelković and Ristić (Andjelković and Ristić, 2015; Pejovic, 2015) implemented phototransistors for gamma radiation detection. Other groups of researchers (Hofstetter *et al.*, 2011; Diab, Ibrahim and El-Mallawany, 2013; Zygmanski *et al.*, 2014) have focused on exploiting photovoltaic sensors for medical dosimetry. Additionally, charge-coupled devices (CCDs) / complementary metal-oxide-semiconductors (CMOSs) cameras have also been implemented for Cerenkov luminescence imaging (CLI) in nuclear medicine (Robertson *et al.*, 2009; Chin *et al.*, 2013; Nordstrom *et al.*, 2013), radiotherapy (Roussakis *et al.*, 2015), and biomedical sciences (Tanha, Pashazadeh and Pogue, 2015; Ciarrocchi and Belcari, 2017).

1.2 Research Problem

As a consequence of radiation-induced damages (Johnston, 2001; Omar *et al.*, 2012b, 2012a; Ali, Khan and Mat Jafri, 2013), the performance of current photonic devices executed for radiation quantification deteriorates upon repeated implementation. Radiation-induced damages may be in the form of post-irradiation lattice structure displacements, post-irradiation dark currents, and post-irradiation sensitivity loss. Performance deterioration ultimately leads to photonic device output degradation (Lischka *et al.*, 1993; Orlova, Gradoboev and Asanov, 2012; Nikolić and Vasić-Milovanović, 2016). For instance, due to continued exposure of photodetectors to X-rays, calibration problems arise in third generation CT scans using a dynamic X-ray source coupled with a set of dynamic photodetectors (Heverhagen, 2016). This is because radiation-induced damages necessitate CT photodetector recalibration to ensure consistent sensitivity every after continued X-ray exposures.

To avert the calibration problems, fourth generation CT scans employ a 360° ring stationary detector array where radiation is ever incident on newly calibrated detectors (Heverhagen, 2016). Nonetheless, about 4800 detector elements are used for the whole 360° ring (Heverhagen, 2016). Furthermore, these photodetectors (photodiodes) may not be of low-cost and flexible enough.

Even though a light-emitting diode (LED) can sense light, a lot of research has tested LEDs in a luminary mode, e.g., in phototherapy and photodynamic therapy (PDT) (Gudgin, Goyan and Pottier, 2002; Dolmans, Fukumura and Jain, 2003). To this end, some research has examined LEDs for sensing light and ultraviolet rays (Murray *et al.*, 2019). However, there is currently limited research that has explored LED response to medical radiation such as diagnostic X-rays. Moreover, LEDs fabricated from materials including gallium nitride (GaN), silicon carbide (SiC) and

amorphous silicon (a-Si:H) could be characterized with better radiation hardness, in comparison to other photonic devices such as photodiodes (Beringer *et al.*, 1999; Dowell *et al.*, 1999; Sellin and Vaitkus, 2006). Particularly, GaN (an element widely implemented in the manufacture of LEDs (Richert, 2020)) has been proposed as more radiation hard, when compared to silicon (Si), a-Si:H, SiC, amorphous SiC (a-SiC), and GaAs (Wang *et al.*, 2015). LED radiation hardness could imply that LEDs may withstand higher radiation doses without any (or with less) read-out degradation, when operated as radiation detectors. This could be a possible alternative that could be applied to avert the current calibration problems in CT scans and other diagnostic radiology detectors. Also, LEDs in the form of surface mount devices (SMD) or chip on board (COB) are flexible and five/three times cheaper than photodiodes (Bryant, 2014a).

As a luminary, current connected across LED terminals excites electrons, localized in valence energy bands, to conduction energy bands. Upon de-excitation (decay), electrons fall back to the valence bands by emission of light photons whose energy is equivalent to the energy band gap (Gayral, 2017).

Similar to photodiodes, LED active regions are predominantly composed of PN junctions (Stokes *et al.*, 2005). When EMR impinges on an LED PN junction, electrons (in the N region) absorb the EMR photons (energy packets) thus drift towards holes (in the P region). Electron drift denotes a quantifiable current. This current could be related to the EMR inducing it. In this thesis, this current was quantified by a multimeter connected across the LED terminals. The multimeter comprised current-to-voltage converters, i.e., operational amplifiers, thus displayed the output signal in volts (V). Therefore, current–voltage (C–V) signal represents the current signals quantified in the form of voltage in this thesis. Hence, exploring radiation hard LEDs

for radiation detection could demonstrate LEDs as an alternative to photodiodes. For instance, radiation hard LEDs could be a possible solution to performance deterioration and calibration problems induced by radiation damages.

1.3 Study Objectives

In general, this thesis aims at exploring and developing an LED based detector system to be implemented for dosimetry in general radiography. LEDs are profoundly fabricated for luminescence. Hence, LEDs are rather optimized for light emission than detection. In the process of reassigning LEDs from emitting light to detecting diagnostic X-rays and light (in the form of a dosimetric system), this thesis aims to:

1. Investigate the LED current-voltage response to (a) diagnostic X-rays (using the cold white, warm white, red, green, and blue LED strip colors), and (b) radiotherapeutic electron and photon beams (using the cold white LED strip).
2. Amplify the diagnostic X-ray-induced current-voltage signal of the cold white LED strip and compare its detection performance to that of the bpw34 photodiode.
3. Design, fabricate, and characterize an LED prototype using beam qualities and quantities.

Successful fabrication of this prototype could demonstrate a possibility of applying LED technology as low-cost X-ray detectors. Eventually, LEDs could be alternatives to photodiodes that are currently implemented for mainly detecting diagnostic X-rays.

1.4 Scope of the Study

This study generally covers photonic devices that modern technology is manipulating for medical radiation detection and dosimetry. The photonic devices encompassed herein include photodiodes, LEDs, phototransistors, photovoltaic sensors, and cameras. Among these photonic devices, focus is emphasized on photodiodes. This is because current literature has immensely exploited photodiodes, and conclusively proposed them as potential alternative radiation detectors.

The present study specifically explores LEDs. LEDs are reverse-function photodiodes. Even though LEDs are luminaries, they could be characterized with a detection response comparable to, or even better than that of photodiodes in terms of radiation hardness. While exploring the execution of LEDs as X-ray detectors, other techniques and methodologies are also executed. Some of these methods include amplification of LED signals using an amplifier board, and by increasing the number of LED chips. Other techniques also include conversion of X-rays to light using a plastic scintillator and an intensifying screen. X-ray to light conversion was intended to optimize X-ray detection and dosimetry by the LEDs. This was because the LEDs are more sensitive to visible light than X-rays, when applied in detector mode.

1.5 Thesis Outline

The function reassignment of LEDs to radiation detection, in this thesis, was executed in different steps. Initially, the surface mount device (SMD) was selected as the shape and type of LEDs to be implemented in this thesis.

In the first stage, five colors of SMD LED strips were selected (cold white, warm white, red, green, blue), and subjected to diagnostic radiology X-rays. This was to determine the LED strip color that could demonstrate the most potential to detect diagnostic X-rays, based on the dosimetric parameters examined.

Upon achieving cold white as the best color, it was unclear whether this LED color could also present the same dosimetric performance when exposed to radiotherapeutic beams. Thus, in the second stage of this study, the cold white LED strip was preliminarily exposed to radiotherapy photon and electron beams. However, the dosimetric response to diagnostic X-rays was better than that to radiotherapeutic beams. Even though the dosimetric response by the cold white LED strip to diagnostic X-rays was good, the signals that were generated were of a low magnitude.

Therefore, in this study's third stage, the signals generated by the cold white LEDs were amplified by increasing the effective detecting active area (number of LED chips) and by injecting the raw signals into an amplifier board with adjustable gains.

As will be elaborated by the literature in CHAPTER 2, the bpw34 photodiode has been implemented most for diagnostic radiology X-ray detection. Thus, in the fourth stage, the dosimetric performance of the cold white LED was compared to that of the bpw34 photodiode. This was to examine whether both these photonic devices would be associated with the same dosimetric characterization, when exposed to similar diagnostic X-ray conditions. Upon execution, both photonic devices were

presented with similar dosimetric properties. This demonstrated the cold white LED as a potential dosimetric device.

Therefore, in the final stage, a prototype employing the cold white LED was designed and characterized for dosimetry applications in diagnostic radiology, by for instance using standard calibration beams.

1.6 Research Study Overview

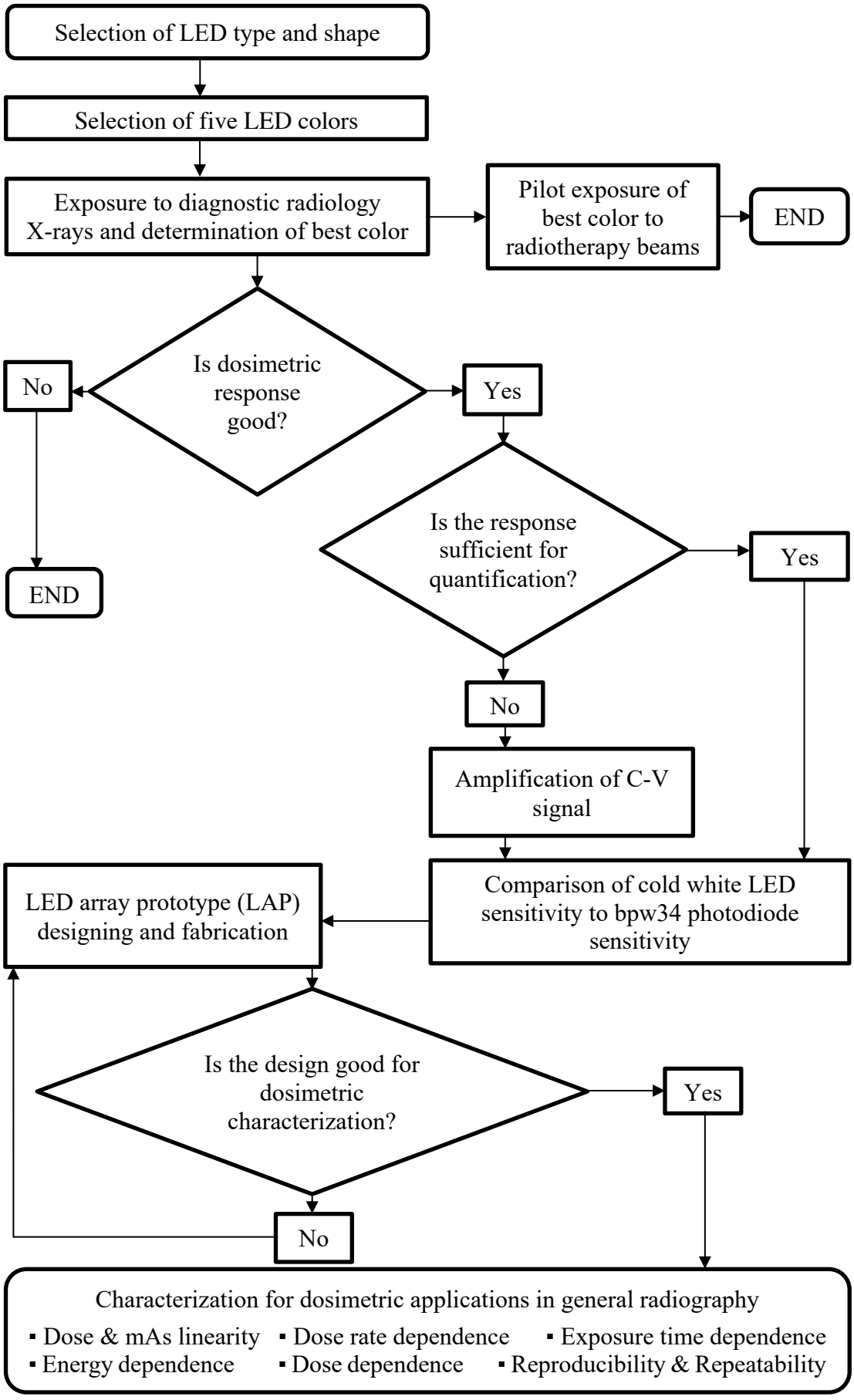

CHAPTER 2

LITERATURE REVIEW

2.1 Electromagnetic Radiation

An electromagnetic wave is a wave that is composed of an electric field component at right angles to a magnetic field component (Khan and Gibbons, 2014). An electromagnetic spectrum (EMS) is a classification of electromagnetic radiation according to wavelength and photon energy.

In the EMS, waves with the shortest wavelength (such as gamma and X-rays) are situated on the far left of the spectrum, whereas those with long wavelengths (e.g., radio and microwaves) are situated on the far right of the EMS. In other words, the wavelength of the waves in the EMS increases while moving from left to right.

The wave-particle duality in quantum mechanics depicts electromagnetic radiation (EMR) simultaneously as a wave and a particle. Thus, EMR is in the form of individual wave packets known as photons (Dance *et al.*, 2014). Therefore, EMR could also be classified in terms of the energy possessed by the individual photons of an EMR. EMR photon energy (E) is defined by (Dance *et al.*, 2014);

$$E = h\nu \tag{2-1}$$

where h is the Plank's constant, and ν is the frequency of the EMR wave. The frequency of an EMR is the number of complete oscillations performed by the wave in a unit time (Dance *et al.*, 2014). The unit for EMR energy (E) is *electron volt* (eV), which is the energy possessed by an electron after being accelerated by a potential difference of 1 volt (Dance *et al.*, 2014).

In this event, EMR whose individual photons possess high amounts of energy such as gamma and X-rays appears on the far left of the EMS. EMR with low amounts

of energy (e.g., radio and microwaves) is on the far right of the EMS, as observed in Figure 2.1 below. Increase in photon energy implies increase in the frequency of the EMR.

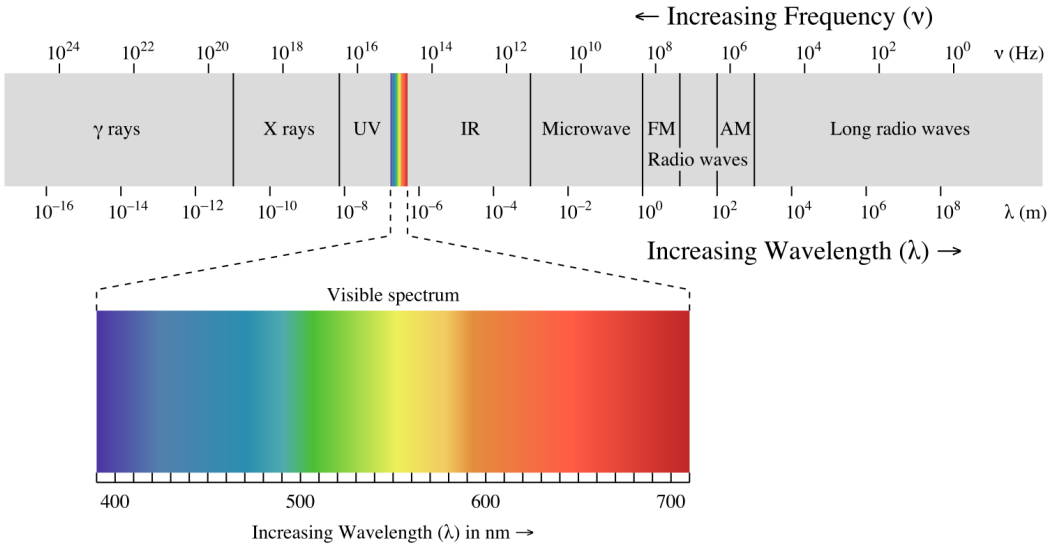

Figure 2.1 The electromagnetic spectrum (reused from (Zedh, 2007)).

In medicine, specific X-ray energy ranges are employed for clinical implementations. For instance, diagnostic imaging procedures that include mammography could use 14 – 25 keV X-ray beams (Correa, Vivolo and Potiens, 2011), yet others such as CT imaging execute energies in the 100 keV range (Dilmanian, 1992). In radiotherapy, MV range X-rays are implemented. Thus, X-rays could be medically applied for diagnostic or therapeutic purposes.

2.2 Medical Radiation

Medical radiation refers to the section of the EMS that is implemented for diagnosis and treatment of human disease. In this case, the X-ray section of the EMS is exploited in diagnostic radiology (diagnostic medical radiation implementation) and

radiotherapy (radiotherapeutic medical radiation implementation). However, in a broader perspective, medical radiation could also include the sound waves of the EMS that are implemented for diagnosis in ultrasonography.

2.2.1 Diagnostic X-rays

Diagnostic X-rays are X-rays that are employed in medicine to diagnose disease. Diagnosis of disease is based on images taken with X-rays. The diagnosis is by comparing X-ray images of healthy and diseased anatomic structures.

Typical diagnostic X-ray photons possess energy ranges from ~ 100 eV to ~ 100 KeV. X-rays in the ~100 eV – 10 keV range could be termed as soft X-rays, whereas those having energies between ~10 keV and 100 KeV as hard X-rays. Wavelength wise, soft X-ray wavelengths range from 10 nm – 100 pm while hard X-rays range between 100 pm and 10 pm (Khan and Gibbons, 2014).

2.2.1 (a) X-ray Generator

In reference to Figure 2.2 (a) , a small current (in milliamperes – mA) flows through the X-ray tube's cathode filament (Hendee, Chaney and Rossi, 1977). A product of the mA and the X-ray beam exposure time (s) is defined as *mAs*. Owing to the resistance against current flow in the cathode filament, the cathode filament is heated up. This results into *thermionic emission* of electrons from the cathode filament (Khan and Gibbons, 2014). The cathode is made of tungsten because tungsten is a good thermionic emitter, has a very high melting point (3,370°C), and is of a high atomic number (A:184, Z:74) (Khan and Gibbons, 2014).

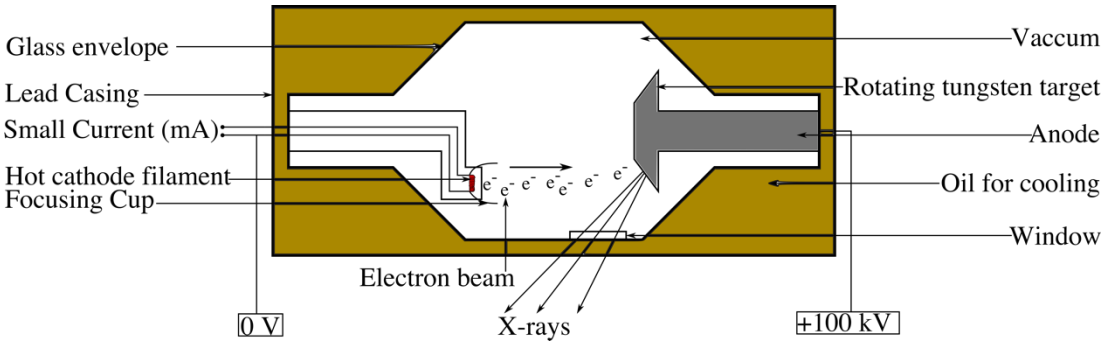

(a)

(b)

Figure 2.2 (a) X-ray production in an X-ray tube, (b) A radiology suite housing a static medical X-ray tube (Q-Rad System, Quantum Medical Imaging, USA).

Proceeding thermionic emission, the electrons drift towards the positive anode on the opposite side of the tube. The movement of these electrons will, however, be at slow speeds since there will be no force to accelerate them to the anode. Additionally, their drifting speeds will be slowed down by collisions with some air particles that could

still be present. Electron beam – air particle collisions are minimized by hermetically sealing the X-ray compartment in a vacuum (Khan and Gibbons, 2014). Thus, a kilo voltage (kV) range potential difference is applied between the anode and the cathode to accelerate the electrons to the anode at very high velocities.

When the electrons strike the tungsten anode surface, there will be X-ray emission by two phenomena namely, bremsstrahlung and K-shell emission. Upon collision, 99 % of the incident electron beam energy is converted to heat and only 1% to X-rays (Bushberg, 2002; Mayles, Nahum and Rosenwald, 2007; Khan and Gibbons, 2014). Therefore, tungsten anodes have a very high melting point (3,370°C) in order to withstand the heating effects (Khan and Gibbons, 2014). Also, the tungsten anode is embedded in a copper substrate that conducts the heat away.

Furthermore, as elaborated in Figure 2.2 (a), the whole X-ray unit is submerged in an oil bath to facilitate cooling. The oil reservoir additionally insulates the tube housing from the high voltage potentials applied across the X-ray unit (Khan and Gibbons, 2014).

2.2.1 (b) Characteristics of X-rays

There are two types of diagnostic X-rays. These include Bremsstrahlung radiation (emission) and characteristic radiation (K-shell emission).

2.2.1 (b) (i) Bremsstrahlung emission

According to Bohr's model of an atom, negatively charged electrons revolve, in shells (tracks), around a highly positive nucleus. The nucleus is composed of positively charged protons and neutrons with zero charge. Both the protons and neutrons also constitute fundamental subatomic particles known as *quarks* (Khan and Gibbons,

2014; Cerrito, 2017). The upward facing quarks possess a charge of $\left(+\frac{2}{3}\right)$ whereas the downward facing quarks possess a charge of $\left(-\frac{1}{3}\right)$ (Khan and Gibbons, 2014). Therefore, protons have two upward and one downward facing quarks hence a net charge of $+1$, i.e., $\left(\frac{2}{3}+\frac{2}{3}-\frac{1}{3}\right)=+1$. On the other hand, neutrons have two downward and one upward facing quarks hence a net charge of zero, i.e., $\left(\frac{2}{3}-\frac{1}{3}-\frac{1}{3}\right)=0$.

Bremsstrahlung radiation is emitted when an accelerated incident electron beam (negatively charged) is slowed down by the attraction forces (Coulombic forces) of the highly positive anode nucleus of the tungsten target (Khan and Gibbons, 2014). In other words, the electron beam brakes (slows) down hence its name *braking radiation*. The energy and direction of bremsstrahlung beams in dependent on the energy of the incident electron beam (Khan and Gibbons, 2014) , as shown in Figure 2.3.

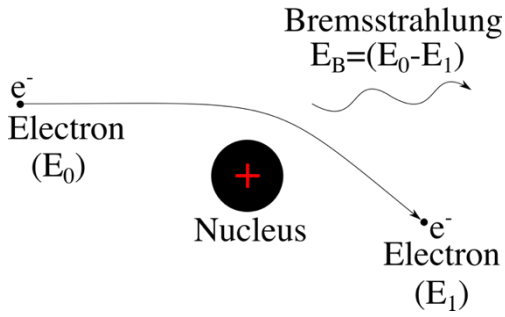

Figure 2.3 Bremsstrahlung radiation emission

In case the final energy of the electron (E_1) approaches zero, as a consequence of repetitive interactions, the bremsstrahlung photon energy (E_B) could become equivalent to the initial electron energy (E_0) (Khan and Gibbons, 2014).

2.2.1 (b) (ii) K-shell emission

This emission occurs when the incident electron plucks out an electron from the innermost tungsten atomic shell (K-shell), as illustrated in Figure 2.4. Electron plucking only occurs when the incident photon's energy is above a threshold energy known as *critical absorption energy* (Khan and Gibbons, 2014). This critical absorption energy could, in other terms, be referred to as the *ionization potential* (Dance *et al.*, 2014). Electrons prefer stability and hence, electrons in higher energy levels (L, M, N) replace the displaced electron in the K-shell. As these electrons cascade to lower energy shells, they emit an X-ray radiation known as K-shell emission (Bushberg, 2002; Dance *et al.*, 2014; Khan and Gibbons, 2014).

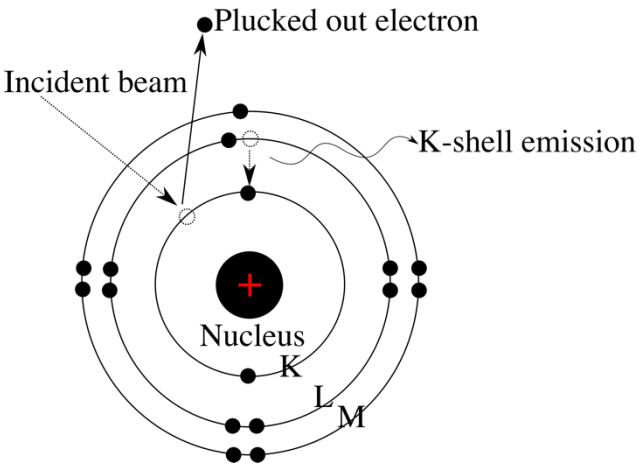

Figure 2.4 K-shell emission

Because electrons drift from one shell to another, K-shell energy values are discrete, unlike bremsstrahlung radiation (Khan and Gibbons, 2014). For instance, a K-shell emission possess an energy (E_K-E_L) when an electron dropped from the L to the K shell.

2.2.2 Therapeutic Photon and Electron Beams

X-ray photon and electron beams utilized for radiotherapeutics are of megavoltage range energies, e.g., 6 and 9 MV or MeV beams. The difference in the energy of X-ray photon and electron beams deployed for diagnostic and radiotherapy purposes is attributed to the modus operandi of the X-ray generation equipment (clinical linear accelerator).

2.2.2 (a) Linear Accelerator (LINAC)

The production mechanism of radiotherapeutic X-rays is similar to that of diagnostic X-rays. In both mechanisms, X-rays are emitted when an accelerated electron beam bombards a target anode.

Radiotherapeutic X-rays are generated by a linear accelerator (LINAC/linac), as shown in Figure 2.5 (a).

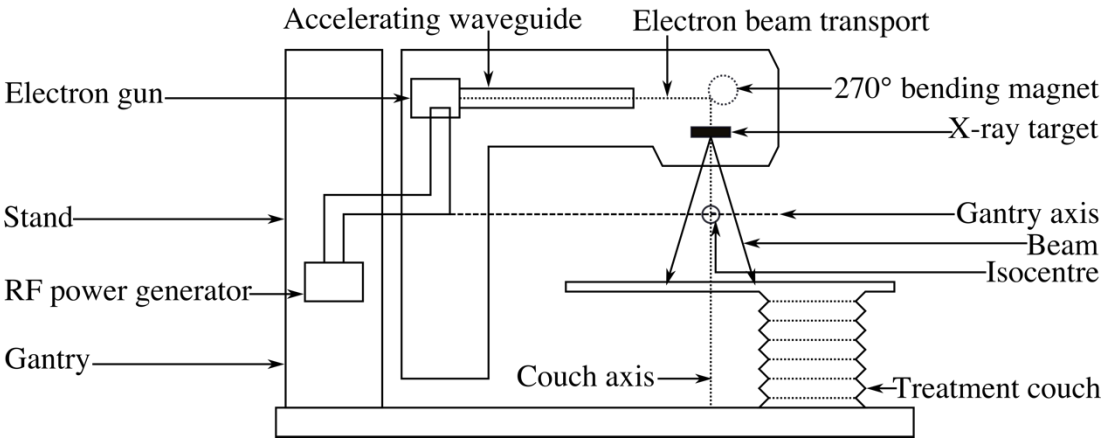

(a) Continued

Figure 2.5 (a) Schematic of X-ray production in a medical linear accelerator, (b) A radiotherapy treatment bunker housing the medical linear accelerator (Primus model 3347, Siemens, Germany).

(b)

Figure 2.5 (Continued) (a) Schematic of X-ray production in a medical linear accelerator, (b) A radiotherapy treatment bunker housing the medical linear accelerator (Primus model 3347, Siemens, Germany).

An electron gun emits electrons (electron beam) like the cathode filament in a diagnostic X-ray tube. The electron gun also comprises a tungsten cathode filament. In a diagnostic X-ray tube, an electron beam is accelerated towards the anode target using an accelerating potential (tube voltage). However, in a linac, electron beam acceleration is performed by radiofrequency waves (RFWs) (microwave region of the EMS) (Khan and Gibbons, 2014). The radio waves could be in motion or stationary and their frequency range is ~ 3,000 megacycles/s (MHz) (Khan and Gibbons, 2014). The RFWs are generated and injected into the waveguide by a radio frequency (RF) generator (magnetron). The magnetron's injection of RFWs into the waveguide is synchronized with the injection of electrons into the waveguide by the electron gun (Khan and Gibbons, 2014). The electron gun propels the electrons into the waveguide with an initial energy of ~ 50 keV. (Khan and Gibbons, 2014). Thereafter, the RFWs

accelerate the electrons to a speed approaching the speed of light. Analogous to a surf rider, the electrons are accelerated while riding on top of the electromagnetic waves, thus gain energy from the sinusoidal electric field. At the end of the end of the waveguide, electrons attain energies about 6 MeV.

When the accelerated electron beam strikes a tungsten anode target, radiotherapeutic X-ray beams are generated. The beam transport system (made of bending magnets, focusing coils and other parts) bends the electron beam through 270°/90° (Khan and Gibbons, 2014) to ensure that the electron beam impinges on the target perpendicularly. In diagnostic radiology, the accelerating (tube) potential influences the energy of the X-ray beams generated. Similarly, radiotherapeutic X-rays possess comparatively very high energies because the electron beam acceleration by the RFWs approaches the speed of light. Therefore, in radiotherapy, X-ray beam energy is adjusted by the magnetron (RF generator). In diagnostic radiology, X-ray beam energy is adjusted by the tube voltage (kVp).

2.2.2 (b) Characteristics of Beams

In the implementation of LINAC-based X-rays, the type and energy of the beams could be selected and implemented according to the size and location of the tumor to be irradiated (treated). For instance, using computer-based treatment planning systems, the beam type (electron or photon) and energy (kV or MV) is selected.

Upon implementation of electron beams, the LINAC retracts the target from the path of the accelerated electron beam, emerging from the electron gun. Thus, the electron beam is directly executed for killing cancerous cells.

Or else, the LINAC's target remains in position and the accelerated electron beam, generated from the electron gun, strikes the tungsten target. Photon beams are

then emitted when the electron beam interacts with the tungsten anode. Thus, the resultant photon beams are also used to kill cancer cells during teletherapy.

2.3 Radiation Detection and Dosimetry

Exposure to ionizing radiation could result into hazardous and adverse effects such as gene mutations and cancerous tumors (Mayles, Nahum and Rosenwald, 2007). Systematic and standard guidelines in the form of *quality assurance* (QA) and *quality control* (QC) are, therefore, implemented to ensure proper medical radiation handling. In medical radiation, QA is a set of guidelines that are put in place to ensure a certain level of quality during the application of radiation in the treatment and diagnosis of human disease (IAEA, 1995, 2009). A QA program involves individual tasks and activities defined as Quality Control; these tasks are performed to implement the QA program (IAEA, 1995). QC includes components such radiation dosimetry.

In simple terms, dosimetry is the quantification and measurement of radiation (Zoetelief *et al.*, 2003). Thus, medical radiation dosimetry is the quantification of the amount of energy deposited into matter (anatomical structure) by ionizing radiation during a medical procedure (Attix, 2008). The energy deposited in a unit mass by ionizing radiation is known as *absorbed dose* (Mayles, Nahum and Rosenwald, 2007). The SI unit for absorbed dose is J/kg (Gray). Absorbed dose (D) (Leroy and Rancoita, 2011; Allisy *et al.*, 2016) is thus derived as;

$$D = \frac{d\bar{\epsilon}}{dm} \tag{2-2}$$

where ϵ is energy and m is mass for the volume V. However, ϵ could be expressed in the form of a stochastic quantity as below (Allisy *et al.*, 2016; Bello, 2017);

$$\epsilon = \mathrm{R_{(in)u}} - \mathrm{R_{(out)u}} + \mathrm{R_{(in)c}} - \mathrm{R_{(out)c}} + \Sigma\, \mathrm{Q} \tag{2-3}$$

where;

$R_{(in)u}$ – total energy from uncharged radiation (particles) entering the volume,

$R_{(out)u}$ – total energy from uncharged radiation (particles) leaving the volume,

$R_{(in)c}$ – total energy from charged radiation (particles) entering the volume,

$R_{(out)c}$ – total energy from charged radiation (particles) leaving the volume, and

ΣQ – the net change in energy arising from the rest mass of a particle inside the volume. Also, ΣQ is defined as (Dance *et al.*, 2014);

$$\Sigma Q = E_{(m \rightarrow R)} - E_{(R \rightarrow m)} \tag{2-4}$$

where $E_{(m \rightarrow R)}$ is the energy change emanating from conversion of particle rest mass to radiant energy $(m \rightarrow R)$. Correspondingly, $(R \rightarrow m)$ implies energy change emanating from conversion of photons to particle rest mass inside the volume V.

In this sense, charged radiation could imply electrons and protons, while uncharged radiation could imply photons and neutrons. When $R_{(in)}$ is defined as the total energy possessed by both charged and uncharged particles entering a volume, and R_{out} as the total energy possessed by both charged and uncharged particles leaving the volume, Equation (2-3) could also be written (simplified) as (McNair, 1981; Allisy *et al.*, 2016) ;

$$\epsilon = R_{(in)} - R_{(out)} + \Sigma Q \tag{2-5}$$

where $(R_{(in)} - R_{(out)})$ is the difference between the energy of the particles entering and leaving the volume. Further, Equation (2-5) is schematically illustrated in Figure 2.6 below.

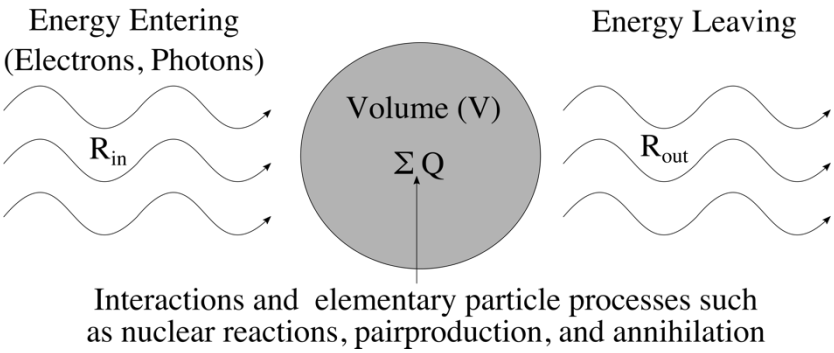

Figure 2.6 Absorbed dose in mass (m) with a volume (V)

In diagnostic radiology, the quantity Σ Q is negligible (Dance *et al.*, 2014). Thus, for diagnostic radiology applications, Equation (2-5) further simplifies to:

$$\epsilon = R_{(in)} - R_{(out)} \tag{2-6}$$

When photons of energy strike matter with mass (m), they liberate charged particles including electrons in this matter. These liberated charges possess kinetic energy (absorbed from the incident photons). The kinetic energy released in matter (by the initially excited charges) is known as KERMA(K). *Kerma* could also be defined as the kinetic energy released per unit mass (energy transferred to a medium). Thus, K is the ratio of dE_{tr} to dm (Mayles, Nahum and Rosenwald, 2007; Dance *et al.*, 2014) i.e.,

$$K = \frac{dE_{tr}}{dm} \tag{2-7}$$

where, dE_{tr} is the total initial kinetic energies of all the charged particles liberated by uncharged particles (indirectly ionizing radiation i.e., photons) in a material of mass dm (Mayles, Nahum and Rosenwald, 2007; Dance *et al.*, 2014).

The unit of kerma is also J/kg (Gy). Therefore, kerma is applicable to indirectly ionizing particles (that do not possess charge) such as photons and neutrons (Mayles, Nahum and Rosenwald, 2007). Although they have the same units, absorbed dose may not be equivalent to kerma. This is because absorbed dose deals with the quantity of

energy deposited into a mass, yet kerma is the initial energy transferred to a mass. With kerma, a fraction of the initial energy transferred to the mass may exit the mass without being actually deposited in the mass (Mayles, Nahum and Rosenwald, 2007). However, in this thesis, the term air kerma would relatively refer to the absorbed dose in air (Sprawls, 1993a).

Absorbed dose is deposited into a mass through interaction mechanisms. Diagnostic and radiotherapeutic X-ray photons, and electron beams interact with anatomical structure particles in the form of coherent collision, photoelectric effect, Compton scattering, and pair production energy transfer mechanisms. However, owing to the relatively higher energies of the radiotherapy beams (MeV/MV), Compton scattering, and pair production are the dominant interaction mechanisms associated with radiotherapy beams.

During Compton scattering, the incident photon possesses energy (hv) surpassing the electron's binding energy. Thus, the electron is dislodged from its shell upon absorption part of the incident photon's energy. After, the incident photon is scattered through an angle (θ) from its original path in the form of a scattered photon (as illustrated in Figure 2.7).

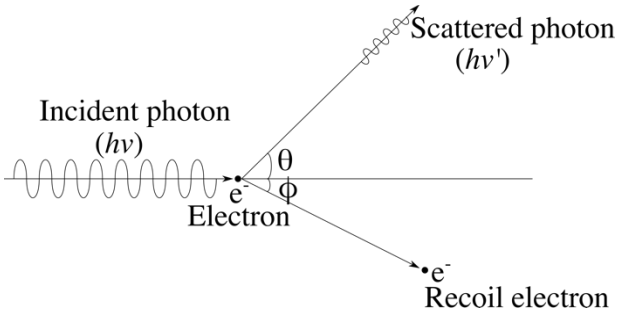

Figure 2.7 Schematic illustrating the geometry of Compton scattering